

# Experimental entanglement swapping through single-photon $\chi^{(2)}$ nonlinearity

Yoshiaki Tsujimoto<sup>1\*</sup>, Kentaro Wakui<sup>1</sup>, Tadashi Kishimoto<sup>1</sup>,  
Shigehito Miki<sup>2,3</sup>, Masahiro Yabuno<sup>2</sup>, Hirotaka Terai<sup>1,2</sup>,  
Mikio Fujiwara<sup>1</sup>, Go Kato<sup>1</sup>

<sup>1\*</sup>National Institute of Information and Communications  
Technology (NICT), Koganei, Tokyo 184-8795, Japan.

<sup>2</sup>National Institute of Information and Communications  
Technology (NICT), Kobe, Hyogo 651-2492, Japan.

<sup>3</sup>Kobe University, Kobe, Hyogo 657-0013, Japan.

\*Corresponding author(s). E-mail(s): [tsujimoto@nict.go.jp](mailto:tsujimoto@nict.go.jp);

## Abstract

In photonic quantum information processing, quantum operations using nonlinear photon-photon interactions are vital for implementing two-qubit gates and enabling faithful entanglement swapping. However, due to the weak interaction between single photons, the all-photonic realization of such quantum operations has remained out of reach so far. Herein, we demonstrate a first entanglement swapping using sum-frequency generation (SFG) between single photons in a  $\chi^{(2)}$ -nonlinear optical waveguide. We show that a highly efficient, stable SFG-based Bell-state analyzer and an ultralow-dark-count superconducting single-photon detector satisfy the high signal-to-noise ratio requirement for the swapping protocol. Furthermore, the system clock is enhanced by utilizing ultrafast telecom entangled photon pair sources that operate in the GHz range. Our results confirm a lower bound 0.770(76) for the swapped state's fidelity, surpassing the classical limit of 0.5 successfully. Our findings highlight the strong potential of broadband all-single-photon nonlinear interactions for further sophistication in long-distance quantum communication and photonic quantum computation.

Nonlinear interactions between independent single photons are key for the advancement of photonic quantum information processing (QIP). The linear-optical elements

have been commonly adopted in the past few decades to configure such systems [1–4]. While these elements involve the use of general optical components, they require a large number of single-photon sources and detectors as the system’s size increases. The configuration of such systems may be dramatically simplified once the nonlinear photon-photon interaction is unlocked. For example, a complete Bell-state measurement (BSM) [5], faithful entanglement swapping [6] and even universal quantum computation [7] can be conducted without the need for complex ancillary systems by exploiting  $\chi^{(2)}$  interaction between single photons. However, the limitations associated with the nonlinear photon-photon interaction have constrained the use in QIP.

A plausible approach to overcome the weak photon-photon nonlinearity is the use of atomic media [8–10], whose feasibility was demonstrated in atom-cavity systems [11–13]. Despite achieving high nonlinearity, the operation of these systems imposes a single longitudinal mode, restricting the wavelength and bandwidth of single photons. This entails the use of the continuous-wave (CW) regime. Nonlinear optical crystals engender the flexibility of designing tailored interacting wavelengths and bandwidths, which caters to applications in broadband quantum communications. Nonlinear optical crystals have enabled several applications of single-photon nonlinearity, including cascaded spontaneous parametric down-conversion (SPDC), with a direct generation of photon triplets [14], and Greenberger–Horne–Zeilinger states [15, 16]. Furthermore, sum-frequency generation (SFG) has been reported between a heralded single photon and weak coherent light [17] and between independent heralded single photons [18]. Despite such characteristics, quantum operations have remained challenging mainly due to the dark count noise of the single-photon detector comparable to the SFG signal. Consequently, no quantum operations using SFG between genuine single photons have been achieved thus far, highlighting the need for higher-efficiency generation and lower-noise detection of SFG photons.

In this study, we address the signal-to-noise ratio (SNR) problem and demonstrate an original entanglement swapping experiment based on SFG between two independent color-distinct single photons. We use a high-efficiency SFG-based Bell-state analyzer (SFG-BSA) unit, which performs the BSM in the polarization degree of freedom (DOF) with the help of  $\chi^{(2)}$  nonlinearity. Our experimental setup features a long periodically-poled lithium niobate waveguide (PPLN/W) [19] within a stable Sagnac interferometer for the SFG-BSA, and a ultralow-dark-count-rate superconducting nanowire single photon detector (SNSPD) optimized for near-infrared detection [20]. Unlike systems that use Mach–Zehnder interferometers (MZIs), an active stabilization is not required in our SFG-BSA unit, enduring weeks-order long-term data acquisition. Moreover, we employ SPDC-based high-repetition-rate telecom entangled photon pair sources (EPSs) [21] tunable in the GHz range to boost the generation rate of input entangled photon pairs.

First, we perform a quantum-teleportation experiment to assess our SFG-BSA unit. We prepare a weak coherent pulse at the single-photon level and an entangled photon pair as an input state. Then, we confirm the SFG-BSA high-fidelity operation by teleporting the polarization state of the weak coherent pulse using the detection signal of the SFG photon for heralding. Subsequently, we conduct the SFG-based

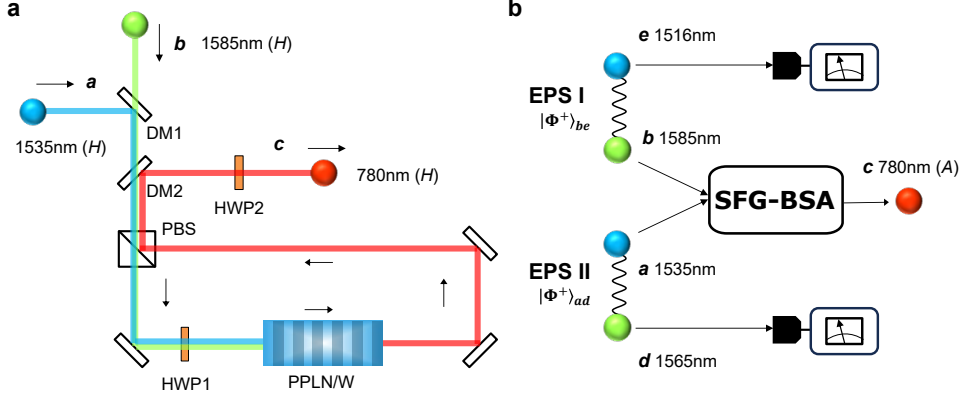


**Fig. 1 SFG-BSA and SFG-based entanglement swapping.** **a**, Schematic of the SFG-BSA, showing the operation for two  $H$ -polarized input photons  $a$  and  $b$ , which are combined into a single spatial mode by dichroic mirror 1 (DM1). They transmit through a polarization beamsplitter (PBS). Then, they flip to  $V$  polarization by half waveplate 1 (HWP1). At the PPLN/W, the  $V$ -polarized photons  $a$  and  $b$  are converted to a  $V$ -polarized single photon  $c$  via the SFG process. Finally, the SFG photon is extracted by DM2, and its polarization is flipped back to  $H$ -polarization by HWP2. **b**, Schematic of the SFG-based entanglement swapping. Detection of a  $D$ -/ $A$ -polarized SFG photon  $c$  at 780nm heralds a creation of entanglement between photons  $d$  and  $e$ .

entanglement swapping experiment using two entangled photon pairs and the SFG-BSA. To our knowledge, this study is the first to realize a quantum operation using SFG between genuine single photons.

## Results

### The SFG-BSA configuration

Figure 1a shows a schematic of the SFG-BSA setup. A type-0 PPLN/W is incorporated in a Sagnac interferometer to extract two of the four Bell states in polarization DOF. It should be noted that this DOF was preferred over time DOF as the latter incurs photon losses by configuring the measurement system with a passive Franson interferometer [22]. In contrast to MZI-based configurations [16], our SFG-BSA does not require phase stabilization between horizontally ( $H$ -) and vertically ( $V$ -) polarized photons. Thus, it can be viewed as a time-reversal of the polarization-entangled photon pair generation using a Sagnac type EPS with a PPLN/W [21, 23, 24]. In this configuration (Fig. 1a), no SFG photon is produced if the two input photons are  $H$ - and  $V$ -polarized, respectively. However, if both input photons are  $V$ -( $H$ -)polarized, they propagate clockwise (counterclockwise) through the interferometer to produce  $V$ -( $H$ -)polarized SFG photons. This can be further discussed through the interaction Hamiltonian:

$$\hat{H} = i\hbar\chi(\hat{a}_H\hat{b}_H\hat{c}_H^\dagger + \hat{a}_V\hat{b}_V\hat{c}_V^\dagger) + \text{H.c.}, \quad (1)$$

where  $\hat{a}_k$  and  $\hat{b}_k$  are annihilation operators of single photons with polarization  $k \in \{H, V\}$  in the input modes  $a$  and  $b$ , respectively,  $\hat{c}_k$  is an annihilation operator of a  $k$ -polarized single photon in the output mode  $c$ , H.c. is the Hermitian conjugate, and  $\hbar$  is the Dirac's constant. Here,  $\chi \in \mathbb{R}$  is a coupling constant that includes the nonlinear susceptibility of PPLN/W, and it is assumed to be independent of the input photons' polarization. Additionally, we assume that the sum of the photon numbers in the input modes  $a$  and  $b$  does not exceed two, and we consider only the lowest order of  $\chi$ . These assumptions are made to describe the ideal operation of the SFG-BSA. The more realistic situations including polarization dependency of  $\chi$  and multi-photon inputs are considered in Theoretical analysis in Methods section. In the case where one photon is generated in mode  $c$  as a success event, the corresponding Kraus operator is given by

$$\hat{K} := \sqrt{\eta_{\text{SFG}}}(|H\rangle_c \langle HH|_{ab} + |V\rangle_c \langle VV|_{ab}), \quad (2)$$

where  $\eta_{\text{SFG}} := (\chi\tau)^2$  and  $|k\rangle_a := \hat{a}_k^\dagger |\text{vac}\rangle$  for  $k \in \{H, V\}$  and so on. Here,  $\tau$  is the traveling time of the input photons through the nonlinear medium and  $|\text{vac}\rangle$  is a vacuum state. By detecting a diagonally ( $D$ -) or anti-diagonally ( $A$ -) polarized SFG photon  $c$  (defined by  $|D\rangle_c = (|H\rangle_c + |V\rangle_c)/\sqrt{2}$  and  $|A\rangle_c = (|H\rangle_c - |V\rangle_c)/\sqrt{2}$ ), the projection on a Bell state  $|\Phi^+\rangle_{ab} := \frac{1}{\sqrt{2}}(|HH\rangle_{ab} + |VV\rangle_{ab})$  or  $|\Phi^-\rangle_{ab} := \frac{1}{\sqrt{2}}(|HH\rangle_{ab} - |VV\rangle_{ab})$  will be respectively performed, which corresponds to a quantum parity check. Compared to a linear-optical BSA [2, 3, 24–27], the SFG-BSA offers the following benefits. First, it aids faithful entanglement swapping based on probabilistic photon pair sources such as SPDC [6], which is applicable for device-independent quantum key distribution [28]. Interestingly, this principle enables tolerance against optical loss for entanglement swapping with the probabilistic sources. Second, by adding another SFG-BSA for odd parity inputs, it enables a complete BSM that distinguishes the four Bell states without employing ancillary systems [5]. Finally, it permits entangling operations between different-color photons, which is useful for building multiuser entanglement networks [29].

Figure 1b describes the entanglement swapping experiment based on the SFG-BSA. The entangled photon pair source I (EPS I) and EPS II generate two maximally entangled photon pairs  $|\Phi^+\rangle_{ad} \otimes |\Phi^+\rangle_{be}$ , while the SFG-BSA is performed on the photons in modes  $a$  and  $b$ , yielding  ${}_c\langle D(A)|\hat{K}|\Phi^+\rangle_{ad} \otimes |\Phi^+\rangle_{be} \propto |\Phi^{+(-)}\rangle_{de}$ , respectively. The overall success probability is  $\sum_{l \in \{D, A\}} |{}_c\langle l|\hat{K}|\Phi^+\rangle_{ad} \otimes |\Phi^+\rangle_{be}|^2 = \eta_{\text{SFG}}/2$ . The experimental success probability is  $\eta_{\text{SFG}}/4$  considering that only one of the  $D$ - or  $A$ -polarized portions is measured.

## Robustness of SFG-BSA against optical losses

To see the loss tolerance of the SFG-BSA with probabilistic sources, we consider an error event of the lowest order, where two photon pairs are generated by EPS I and one photon pair is generated by EPS II in the entanglement swapping. Two types of fake success events may occur at the BSA, and they may subsequently degrade the swapped state's SNR. First, two photons (i.e., one from each EPS) arrive at the BSA, which results in a coincidence detection. Second, one photon from EPS II is lost before the BSA, and a coincidence detection is induced by two photons from EPS I. The first

event commonly occurs in the linear-optical BSA and SFG-BSA. The second event can be excluded when using the SFG-BSA. Let  $\gamma^2$  be the respective photon pair generation probability of EPS I and EPS II, and let  $T$  be the transmittance of each communication channel. Then, the probability of the second event is given by  $p_f \propto \gamma^6 T^2 (1 - T)$ . Because the probability of the true success event is given by  $p_s \propto \gamma^4 T^2$ , the ratio is calculated as  $p_f/p_s = \gamma^2 (1 - T)$ . This indicates that the portion of the fake success event is proportional to the optical loss  $(1 - T)$ . Nevertheless, it is possible to exclude such an event in the SFG-BSA case because SFG occurs only when at least one photon arrives from each EPS. Here, the second harmonic generation (SHG) between the two photons from EPS I is set beyond the phase-matching condition of the nonlinear crystal. Additionally, the SFG photon-detection system is configured such that it does not detect the SHG photons, and this results in an increase in the robustness of the SFG-BSA against optical loss. The quantitative analysis is given in S1 and S2 in Supplementary information.

## Experiment

### SFG-BSA unit

The SFG-BSA unit consists of a home-built type-0 MgO-doped PPLN ridge waveguide (PPLN/W3) with free space coupling (length: 6.3 cm). To estimate the single-photon SFG efficiency, we used coherent light pulses centered at 1535 and 1585 nm. These pulses are generated according to the difference frequency generation (DFG) at EPS I and II with the addition of CW laser light at 1565 and 1516 nm, respectively. Their coupling efficiencies to the PPLN/W3 were measured to be 0.77 and 0.89, respectively, indicating a large mode matching between the input-photon and waveguide modes. By measuring the average power of the DFG pulses and the count rate of the SFG photons, the internal SFG conversion efficiency for single-photon inputs can be estimated as

$$\eta_{\text{SFG}} = \frac{C_{\text{SFG}}}{\eta_T \eta_d f} \times \frac{hc f}{P_a \lambda_a} \times \frac{hc f}{P_b \lambda_b}, \quad (3)$$

where  $c$  is the speed of light,  $h$  is the Planck's constant,  $\eta_T$  and  $\eta_d$  are the transmittance and quantum efficiency of the single-photon detector for the SFG photons, respectively. Further,  $P_{a(b)}$  and  $\lambda_{a(b)}$  are the average power and wavelength of the DFG pulses in modes  $a$  and  $b$ , respectively.  $C_{\text{SFG}}$  is the count rate of the SFG photons, and  $f=1.0$  GHz is the repetition rate of the DFG pulses. Using the experimental parameters summarized in Table. 1, we obtained  $\eta_{\text{SFG}}^H = 2.31 \times 10^{-8}$  and  $\eta_{\text{SFG}}^V = 2.35 \times 10^{-8}$  for  $H$ - and  $V$ -polarized inputs, respectively.

**Table 1 Parameters of the SFG module**

	$C_{\text{SFG}}$	$\eta_T$	$\eta_d$	$P_a$	$P_b$
H	2.54 MHz	0.43	0.85	80 nW	61 nW
V	1.94 MHz	0.40	0.85	70 nW	56 nW

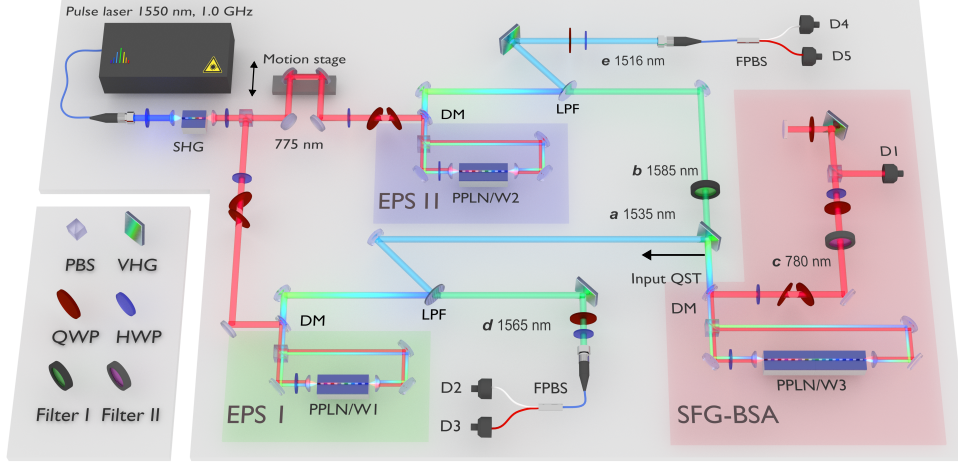


**Fig. 2 Experimental setup for the SFG-based entanglement swapping.** Pump pulses centered at 775 nm with a 1.0-GHz repetition rate is prepared by second harmonic generation (SHG) of the electro-optical (EO) comb centered at 1550 nm and used to pump EPS I and II. Each EPS consists of a PPLN/W in a Sagnac interferometer with a polarizing beamsplitter (PBS). The signal and idler photons at telecom wavelengths are divided into different spatial modes through low pass filters (LPFs). Photon  $a$  at 1535 nm and photon  $b$  at 1585 nm are narrowed by a volume holographic grating (VHG) and band pass filter (Filter I), respectively, and they are fed into the SFG-BSA unit. A flip mirror (not shown) just before the SFG-BSA is used to perform the quantum state tomography (QST) on the input quantum states. The output SFG photon  $c$  at 780 nm passes through the band pass filter (Filter II) and is diffracted twice by a VHG. The polarization of the SFG photon is projected on the  $A$ -polarization by means of a quarter waveplate (QWP), half waveplate (HWP), and PBS. The photon-detection signal from the SNSPD (D1) is used as the start signal of a time-to-digital converter (not shown). Photons  $d$  and  $e$  are diffracted by VHG. The polarization correlation of the swapped state  $\hat{\rho}_{de}$  is evaluated by QWPs, HWPs, and fiber-based PBSs (FPBSs) followed by SNSPDs (D2-D5).

### SFG-based quantum teleportation

To assess our SFG-BSA unit, we performed a quantum-teleportation experiment. The input light to be teleported was generated by performing DFG at EPS II. We prepared  $H$ -,  $A$ -, and right circularly ( $R$ -) polarized weak coherent light as input states, and we set the average photon number as 0.95 per pulse. Then, we reconstructed the density matrices of the input states by conducting quantum state tomography (QST) [30]. Figure 3a shows an example of the density matrix for the  $A$ -polarized state (S3 in Supplementary information for the density matrices of the  $H$ - and  $R$ -polarized input states). The fidelities of the  $H$ -,  $A$ -, and  $R$ -polarized states are  $\langle H | \hat{\rho}_b | H \rangle = 0.97050(9)$ ,  $\langle A | \hat{\rho}_b | A \rangle = 0.99735(3)$  and  $\langle R | \hat{\rho}_b | R \rangle = 0.97500(8)$ , respectively, and here,  $|R\rangle := (|H\rangle + i|V\rangle)/\sqrt{2}$ . The fidelity errors correspond to the standard deviations with the assumption of Poisson statistics for the photon counts. In addition, we prepared an entangled photon pair using EPS I, whose density matrix is shown in Fig. 3b. The fidelity to the ideal state  $|\Phi^+\rangle$  is  $\langle \Phi^+ | \hat{\rho}_{ad} | \Phi^+ \rangle = 0.9163(4)$ . We input the weak coherent light in mode  $b$  and the photon in mode  $a$  into the SFG-BSA. Under the condition that a  $D$ -polarized SFG photon is detected by D1, we performed the

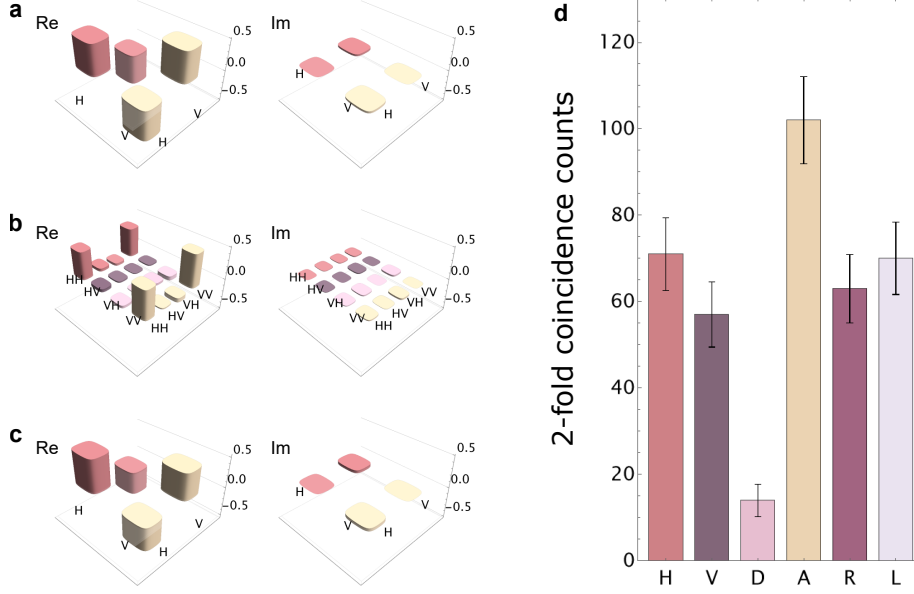


**Fig. 3 Experimental results for the SFG-based quantum teleportation.** **a**, Density matrix of the  $A$ -polarized input state. The left (right) of each plot shows the real (imaginary) part of the density matrix, respectively. **b**, Density matrix of the entangled state. **c**, Density matrix of the teleported state. **d**, Raw counts of the teleported photons for the  $A$ -polarized input light. The measurement time is 13 h for each basis state. Here,  $R$  and  $L$  represent right and left circular polarizations, respectively.

QST on photon  $d$  (see Fig. 2). Figures 3c and 3d show the density matrix of the teleported state and the raw detection counts for the  $A$ -polarized input, respectively. The fidelity is 0.890(30), and the measurement time is 13 h for each basis state. For  $H$ - and  $R$ -polarized inputs, the fidelities are 0.893(28) and 0.840(39), respectively. These values significantly exceed the classical limit of  $2/3$  [31], indicating the high fidelity of the SFG-BSA for inputs at the single-photon level. It is worth noting that the results in Ref. [5] were reported as quantum teleportation using SFG with  $10^{10}$  input photons on average. Nevertheless, these results can be rather understood as a quantum frequency conversion (QFC) [32–34] in the weak pump regime, in contrast to the present quantum-teleportation experiment with single-photon-level inputs. This is because in the situation of Ref. [5], the input light is regarded as the pump light of the QFC. Hence, the quantum-teleportation-like behavior is observed under the condition that the conversion efficiency of the QFC can be approximately regarded as proportional to the average intensity of the input light. In the strong pump regime where the above approximation does not hold, the polarization state is no longer transferred. A detailed discussion is given in S4 in Supplementary information.

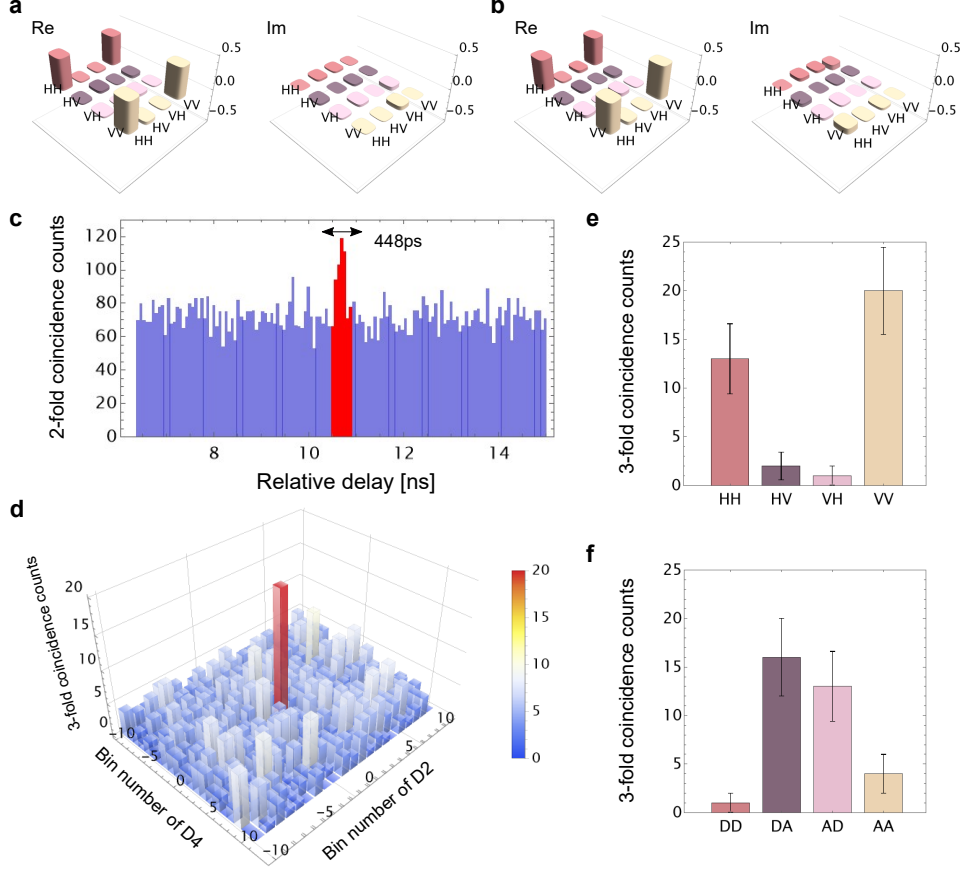


**Fig. 4 Experimental results for the SFG-based entanglement swapping.** **a,b**, Density matrices of the input states from EPS I and II, respectively. **c**, Two-fold coincidence counts between D2 and D4. We employed a 448-ps coincidence window corresponding to seven bins around the signal peak. **d**, Three-fold coincidence counts among D1, D2, and D4. The center bin corresponds to the signal event. The waveplates were set so that D2 and D4 detect *V*-polarized portions of photons *d* and *e*, respectively. The measurement time is 226 h. **e,f**, Raw detection counts of the swapped state for each basis state. The error bars were calculated assuming the Poisson statistics.

### SFG-based entanglement swapping

Figure 2 depicts the experimental setup for the entanglement swapping. We prepared two initial entangled photon pairs  $\hat{\rho}_{ad}$  and  $\hat{\rho}_{be}$  as input states. Their density matrices are shown in Figs. 4a and 4b, respectively. The fidelities are  $\langle \Phi^+ | \hat{\rho}_{ad} | \Phi^+ \rangle = 0.9079(4)$  and  $\langle \Phi^+ | \hat{\rho}_{be} | \Phi^+ \rangle = 0.8775(6)$ . The photons *a* and *b* were combined by a volume holographic grating (VHG) and fed to the SFG-BSA. When an *A*-polarized SFG photon at 780 nm is detected by the SNSPD (D1), the both output ports of the FPBSs are simultaneously measured using SNSPDs D2, D3, D4 and D5. A low-noise detection of the SFG photon *c* was enabled by D1, which possesses a high quantum efficiency ( $\eta_d=85\%$ )



and an ultralow dark count rate ( $R_d = 0.15$  Hz). The typical quantum efficiency of D2, D3, D4 and D5 is 75 %. Figure 4c shows an example of the two-fold coincidence between D1 and D2. We observe a signal peak corresponding to the coincidence detection between photons  $c$  and  $d$ . Background counts are primarily caused by the coincidence between the dark count at D1 and the detection of photon  $d$  at D2. We used a coincidence window of  $\tau_w = 448$  ps, corresponding to seven bins around the signal peak, shown by the red bars in Fig. 4c. The three-fold coincidence histogram among D1, D2, and D4 with bin widths  $\tau_w$  is shown in Fig. 4d. We clearly identify a signal peak corresponding to  $P_{VV} := \langle VV | \hat{\rho}_{de} | VV \rangle$ , with a measured SNR equal to  $5.57 \pm 1.48$ . We perform Z-basis measurements that distinguish the  $H/V$  polarization and X-basis measurements that distinguish the  $D/A$  polarization on photons  $d$  and  $e$ , respectively. Each measurement (30-min duration) was repeated 452 times, resulting in an overall measurement time of 226 h for each basis state. The coincidence counts of the swapped state for eight basis states are shown in Figs. 4e and 4f. The polarization correlation corresponding to the target swapped state  $|\Phi^-\rangle_{de} = (|HH\rangle_{de} - |VV\rangle_{de})/\sqrt{2} = (|DA\rangle_{de} + |AD\rangle_{de})/\sqrt{2}$  is clearly identified. We evaluated the quality of the swapped state by the visibilities for Z-basis ( $V_Z := \langle \hat{Z}_d \hat{Z}_e \rangle$ ) and X-basis ( $V_X := -\langle \hat{X}_d \hat{X}_e \rangle$ ), where  $\hat{Z} := |H\rangle\langle H| - |V\rangle\langle V|$  and  $\hat{X} := |H\rangle\langle V| + |V\rangle\langle H|$ . We observed high visibilities of  $V_Z = 0.833(92)$  and  $V_X = 0.706(121)$ . Although these parameters are not sufficient to reconstruct the complete density matrix, they help estimate the fidelity's lower bound  $F \geq F_{\text{low}} = (V_Z + V_X)/2$  [35, 36]. The experimental value of  $F_{\text{low}}$  was found to be equal to  $0.770(76)$ , which confirms that the swapped state is strongly entangled.

## Discussion

In the present experiment, we have implemented a BSA using SFG between single photons and demonstrated the quantum teleportation and entanglement swapping. We have confirmed the high-fidelity of the teleported/swapped states, which is an important milestone toward QIP using single-photon  $\chi^{(2)}$  nonlinearity. Our method could be used for all-photonic loophole-free Bell tests over long distances and device-independent quantum key distribution [6]. Furthermore, the single-photon SFG is an important building block for implementing a controlled-Z gate in the universal quantum computation [7]. Toward such applications, further improvements in protocol success rates and SNR can be expected by increasing the SFG efficiency and sophistication of EPSs. In recent years, there has been notable progress in the research on the nonlinear optical efficiency of thin-film lithium niobate platforms [37]. In particular, Ref. [38] reports a very high SHG efficiency of 5,000,000 %/W. Such devices can help significantly improve the SNR and success rates if the insertion loss is reduced. Moreover, the frequency multiplexing of the EPSs is highly effective in increasing the success rates. Our EPSs possess a bandwidth of approximately 5.0 THz [21] for each of the signal and idler photons, and approximately 32 GHz of this bandwidth was extracted and used in this experiment. In other words, frequency multiplexing can improve the success rates by a factor of approximately 156. Combined with these technologies, our method provides a new avenue towards all-photonic QIP using the single-photon  $\chi^{(2)}$  nonlinearity.

## Note added

During the preparation of the manuscript presented here, we learned of an experiment demonstrating quantum teleportation using single-photon SFG by Akin *et al.* [39].

**Acknowledgements.** Y. T. thanks Rikizo Ikuta and Toshiki Kobayashi for helpful discussions. This work was supported by Japan Society for the Promotion of Science (JP18K13487, JP20K14393, JP22K03490).

## Declarations

### Data availability

The main data that support the findings of this study are available in this Article and its Supplementary Information. Additional data are available from the corresponding authors upon reasonable request.

### Author contribution

Y.T. conceived the idea, conducted the experiment with K.W. and performed simulation with G.K.. T. K. fabricated a PPLN/W used for the SFG-BSA unit. S. M., M. Y. and H.T. fabricated SNSPDs. All authors discussed the results and contributed to the manuscript.

### Competing interests

The authors declare no competing interests.

## References

- [1] Knill, E., Laflamme, R., Milburn, G.J.: A scheme for efficient quantum computation with linear optics. *Nature* **409**(6816), 46–52 (2001) <https://doi.org/10.1038/35051009>
- [2] Koashi, M., Yamamoto, T., Imoto, N.: Probabilistic manipulation of entangled photons. *Phys. Rev. A* **63**, 030301 (2001) <https://doi.org/10.1103/PhysRevA.63.030301>
- [3] Pittman, T.B., Jacobs, B.C., Franson, J.D.: Probabilistic quantum logic operations using polarizing beam splitters. *Phys. Rev. A* **64**, 062311 (2001) <https://doi.org/10.1103/PhysRevA.64.062311>
- [4] Ralph, T.C., White, A.G., Munro, W.J., Milburn, G.J.: Simple scheme for efficient linear optics quantum gates. *Phys. Rev. A* **65**, 012314 (2001) <https://doi.org/10.1103/PhysRevA.65.012314>
- [5] Kim, Y.-H., Kulik, S.P., Shih, Y.: Quantum teleportation of a polarization state with a complete bell state measurement. *Phys. Rev. Lett.* **86**, 1370–1373 (2001) <https://doi.org/10.1103/PhysRevLett.86.1370>

- [6] Sangouard, N., Sanguinetti, B., Curtz, N., Gisin, N., Thew, R., Zbinden, H.: Faithful entanglement swapping based on sum-frequency generation. *Phys. Rev. Lett.* **106**, 120403 (2011) <https://doi.org/10.1103/PhysRevLett.106.120403>
- [7] Niu, M.Y., Chuang, I.L., Shapiro, J.H.: Qudit-basis universal quantum computation using  $\chi^{(2)}$  interactions. *Phys. Rev. Lett.* **120**, 160502 (2018) <https://doi.org/10.1103/PhysRevLett.120.160502>
- [8] Schmidt, H., Imamoglu, A.: Giant kerr nonlinearities obtained by electromagnetically induced transparency. *Opt. Lett.* **21**(23), 1936–1938 (1996) <https://doi.org/10.1364/OL.21.001936>
- [9] Chuang, I.L., Yamamoto, Y.: Simple quantum computer. *Phys. Rev. A* **52**, 3489–3496 (1995) <https://doi.org/10.1103/PhysRevA.52.3489>
- [10] Duan, L.-M., Kimble, H.J.: Scalable photonic quantum computation through cavity-assisted interactions. *Phys. Rev. Lett.* **92**, 127902 (2004) <https://doi.org/10.1103/PhysRevLett.92.127902>
- [11] Kubanek, A., Ourjoumtsev, A., Schuster, I., Koch, M., Pinkse, P.W.H., Murr, K., Rempe, G.: Two-photon gateway in one-atom cavity quantum electrodynamics. *Phys. Rev. Lett.* **101**, 203602 (2008) <https://doi.org/10.1103/PhysRevLett.101.203602>
- [12] Peyronel, T., Firstenberg, O., Liang, Q.-Y., Hofferberth, S., Gorshkov, A.V., Pohl, T., Lukin, M.D., Vuletić, V.: Quantum nonlinear optics with single photons enabled by strongly interacting atoms. *Nature* **488**(7409), 57–60 (2012) <https://doi.org/10.1038/nature11361>
- [13] Stolz, T., Hegels, H., Winter, M., Röhr, B., Hsiao, Y.-F., Husel, L., Rempe, G., Dürr, S.: Quantum-logic gate between two optical photons with an average efficiency above 40%. *Phys. Rev. X* **12**, 021035 (2022) <https://doi.org/10.1103/PhysRevX.12.021035>
- [14] Hübel, H., Hamel, D.R., Fedrizzi, A., Ramelow, S., Resch, K.J., Jennewein, T.: Direct generation of photon triplets using cascaded photon-pair sources. *Nature* **466**(7306), 601–603 (2010) <https://doi.org/10.1038/nature09175>
- [15] Shalm, L.K., Hamel, D.R., Yan, Z., Simon, C., Resch, K.J., Jennewein, T.: Three-photon energy-time entanglement. *Nature Physics* **9**(1), 19–22 (2013) <https://doi.org/10.1038/nphys2492>
- [16] Hamel, D.R., Shalm, L.K., Hübel, H., Miller, A.J., Marsili, F., Verma, V.B., Mirin, R.P., Nam, S.W., Resch, K.J., Jennewein, T.: Direct generation of three-photon polarization entanglement. *Nature Photonics* **8**(10), 801–807 (2014) <https://doi.org/10.1038/nphoton.2014.218>

- [17] Guerreiro, T., Pomarico, E., Sanguinetti, B., Sangouard, N., Pelc, J.S., Langrock, C., Fejer, M.M., Zbinden, H., Thew, R.T., Gisin, N.: Interaction of independent single photons based on integrated nonlinear optics. *Nature Communications* **4**(1), 2324 (2013) <https://doi.org/10.1038/ncomms3324>
- [18] Guerreiro, T., Martin, A., Sanguinetti, B., Pelc, J.S., Langrock, C., Fejer, M.M., Gisin, N., Zbinden, H., Sangouard, N., Thew, R.T.: Nonlinear interaction between single photons. *Phys. Rev. Lett.* **113**, 173601 (2014) <https://doi.org/10.1103/PhysRevLett.113.173601>
- [19] Kishimoto, T., Inafune, K., Ogawa, Y., Sasaki, H., Murai, H.: Highly efficient phase-sensitive parametric gain in periodically poled LiNbO<sub>3</sub> ridge waveguide. *Opt. Lett.* **41**(9), 1905–1908 (2016) <https://doi.org/10.1364/OL.41.001905>
- [20] Miki, S., Yabuno, M., Yamashita, T., Terai, H.: Stable, high-performance operation of a fiber-coupled superconducting nanowire avalanche photon detector. *Opt. Express* **25**(6), 6796–6804 (2017) <https://doi.org/10.1364/OE.25.006796>
- [21] Wakui, K., Tsujimoto, Y., Fujiwara, M., Morohashi, I., Kishimoto, T., China, F., Yabuno, M., Miki, S., Terai, H., Sasaki, M., Takeoka, M.: Ultra-high-rate non-classical light source with 50 GHz-repetition-rate mode-locked pump pulses and multiplexed single-photon detectors. *Opt. Express* **28**(15), 22399–22411 (2020) <https://doi.org/10.1364/OE.397030>
- [22] Brendel, J., Gisin, N., Tittel, W., Zbinden, H.: Pulsed energy-time entangled twin-photon source for quantum communication. *Phys. Rev. Lett.* **82**, 2594–2597 (1999) <https://doi.org/10.1103/PhysRevLett.82.2594>
- [23] Yamazaki, T., Ikuta, R., Kobayashi, T., Miki, S., China, F., Terai, H., Imoto, N., Yamamoto, T.: Massive-mode polarization entangled biphoton frequency comb. *Scientific Reports* **12**(1), 8964 (2022) <https://doi.org/10.1038/s41598-022-12691-7>
- [24] Tsujimoto, Y., Tanaka, M., Iwasaki, N., Ikuta, R., Miki, S., Yamashita, T., Terai, H., Yamamoto, T., Koashi, M., Imoto, N.: High-fidelity entanglement swapping and generation of three-qubit GHZ state using asynchronous telecom photon pair sources. *Scientific Reports* **8**(1), 1446 (2018) <https://doi.org/10.1038/s41598-018-19738-8>
- [25] Pan, J.-W., Bouwmeester, D., Weinfurter, H., Zeilinger, A.: Experimental entanglement swapping: Entangling photons that never interacted. *Phys. Rev. Lett.* **80**, 3891–3894 (1998) <https://doi.org/10.1103/PhysRevLett.80.3891>
- [26] Halder, M., Beveratos, A., Gisin, N., Scarani, V., Simon, C., Zbinden, H.: Entangling independent photons by time measurement. *Nature Physics* **3**(10), 692–695 (2007) <https://doi.org/10.1038/nphys700>

- [27] Jin, R.-B., Takeoka, M., Takagi, U., Shimizu, R., Sasaki, M.: Highly efficient entanglement swapping and teleportation at telecom wavelength. *Scientific Reports* **5**(1), 9333 (2015) <https://doi.org/10.1038/srep09333>
- [28] Acín, A., Brunner, N., Gisin, N., Massar, S., Pironio, S., Scarani, V.: Device-independent security of quantum cryptography against collective attacks. *Phys. Rev. Lett.* **98**, 230501 (2007) <https://doi.org/10.1103/PhysRevLett.98.230501>
- [29] Li, Y., Huang, Y., Xiang, T., Nie, Y., Sang, M., Yuan, L., Chen, X.: Multiuser time-energy entanglement swapping based on dense wavelength division multiplexed and sum-frequency generation. *Phys. Rev. Lett.* **123**, 250505 (2019) <https://doi.org/10.1103/PhysRevLett.123.250505>
- [30] James, D.F.V., Kwiat, P.G., Munro, W.J., White, A.G.: Measurement of qubits. *Phys. Rev. A* **64**, 052312 (2001) <https://doi.org/10.1103/PhysRevA.64.052312>
- [31] Massar, S., Popescu, S.: Optimal extraction of information from finite quantum ensembles. *Phys. Rev. Lett.* **74**, 1259–1263 (1995) <https://doi.org/10.1103/PhysRevLett.74.1259>
- [32] Kumar, P.: Quantum frequency conversion. *Opt. Lett.* **15**(24), 1476–1478 (1990) <https://doi.org/10.1364/OL.15.001476>
- [33] Tanzilli, S., Tittel, W., Halder, M., Alibart, O., Baldi, P., Gisin, N., Zbinden, H.: A photonic quantum information interface. *Nature* **437**(7055), 116–120 (2005) <https://doi.org/10.1038/nature04009>
- [34] Ikuta, R., Kusaka, Y., Kitano, T., Kato, H., Yamamoto, T., Koashi, M., Imoto, N.: Wide-band quantum interface for visible-to-telecommunication wavelength conversion. *Nature Communications* **2**(1), 537 (2011) <https://doi.org/10.1038/ncomms1544>
- [35] Nagata, K., Koashi, M., Imoto, N.: Observables suitable for restricting the fidelity to multipartite maximally entangled states. *Phys. Rev. A* **65**, 042314 (2002) <https://doi.org/10.1103/PhysRevA.65.042314>
- [36] Ikuta, R., Ono, Y., Tashima, T., Yamamoto, T., Koashi, M., Imoto, N.: Efficient decoherence-free entanglement distribution over lossy quantum channels. *Phys. Rev. Lett.* **106**, 110503 (2011) <https://doi.org/10.1103/PhysRevLett.106.110503>
- [37] Zhu, D., Shao, L., Yu, M., Cheng, R., Desiatov, B., Xin, C.J., Hu, Y., Holzgrafe, J., Ghosh, S., Shams-Ansari, A., Puma, E., Sinclair, N., Reimer, C., Zhang, M., Lončar, M.: Integrated photonics on thin-film lithium niobate. *Adv. Opt. Photon.* **13**(2), 242–352 (2021) <https://doi.org/10.1364/AOP.411024>
- [38] Lu, J., Li, M., Zou, C.-L., Sayem, A.A., Tang, H.X.: Toward 1% single-photon anharmonicity with periodically poled lithium niobate microring resonators.

- Optica **7**(12), 1654–1659 (2020) <https://doi.org/10.1364/OPTICA.403931>
- [39] Akin, J., Zhao, Y., Kwiat, P.G., Goldschmidt, E.A., Fang, K.: Faithful quantum teleportation via a nanophotonic nonlinear bell state analyzer. arXiv:2411.15437 (2024)
- [40] Sakamoto, T., Kawanishi, T., Izutsu, M.: Asymptotic formalism for ultraflat optical frequency comb generation using a mach-zehnder modulator. Opt. Lett. **32**(11), 1515–1517 (2007) <https://doi.org/10.1364/OL.32.001515>
- [41] Jin, R.-B., Shimizu, R., Morohashi, I., Wakui, K., Takeoka, M., Izumi, S., Sakamoto, T., Fujiwara, M., Yamashita, T., Miki, S., Terai, H., Wang, Z., Sasaki, M.: Efficient generation of twin photons at telecom wavelengths with 2.5 GHz repetition-rate-tunable comb laser. Scientific Reports **4**(1), 7468 (2014) <https://doi.org/10.1038/srep07468>
- [42] Tsujimoto, Y., Wakui, K., Fujiwara, M., Sasaki, M., Takeoka, M.: Ultra-fast hongou-mandel interferometry via temporal filtering. Opt. Express **29**(23), 37150–37160 (2021) <https://doi.org/10.1364/OE.430502>
- [43] Wakui, K., Tsujimoto, Y., Kishimoto, T., Fujiwara, M., Sasaki, M., Hosaka, A., Kannari, F., Takeoka, M.: Modelocked thermal frequency combs for ultrashort chaotic quantum optics. Advanced Quantum Technologies, 2400026 (2024) <https://doi.org/10.1002/qute.202400026> <https://onlinelibrary.wiley.com/doi/pdf/10.1002/qute.202400026>
- [44] Klyshko, D.N.: Use of two-photon light for absolute calibration of photoelectric detectors. Soviet Journal of Quantum Electronics **10**(9), 1112 (1980) <https://doi.org/10.1070/QE1980v010n09ABEH010660>
- [45] Ikuta, R., Kobayashi, T., Kawakami, T., Miki, S., Yabuno, M., Yamashita, T., Terai, H., Koashi, M., Mukai, T., Yamamoto, T., Imoto, N.: Polarization insensitive frequency conversion for an atom-photon entanglement distribution via a telecom network. Nature Communications **9**(1), 1997 (2018) <https://doi.org/10.1038/s41467-018-04338-x>
- [46] Bock, M., Eich, P., Kucera, S., Kreis, M., Lenhard, A., Becher, C., Eschner, J.: High-fidelity entanglement between a trapped ion and a telecom photon via quantum frequency conversion. Nature Communications **9**(1), 1998 (2018) <https://doi.org/10.1038/s41467-018-04341-2>
- [47] Leent, T., Bock, M., Garthoff, R., Redeker, K., Zhang, W., Bauer, T., Rosenfeld, W., Becher, C., Weinfurter, H.: Long-distance distribution of atom-photon entanglement at telecom wavelength. Phys. Rev. Lett. **124**, 010510 (2020) <https://doi.org/10.1103/PhysRevLett.124.010510>

# Methods

## Entangled photon pair sources

We employed an electro-optical (EO) frequency comb generator to emit a fundamental pulse to pump SPDC and realized high-speed generation of entangled photon pairs. The setups of EPS I and EPS II are shown on the left side of Fig. 2. We generated an EO frequency comb centered at 1550 nm with a 10-GHz repetition rate by EO phase modulation on the narrow-band CW laser light [21, 40–42]. We reduced it to 1/10 through optical gating [43]. We selected a 1.0-GHz repetition rate such that the SNSPDs can resolve each pulse without saturating. The wavelength of the fundamental pulse was halved by SHG using a 1.0-cm-long PPLN/W. The SHG pulse bandwidth was measured to be 34-GHz full-width at half maximum (FWHM). Each EPS consists of a 3.4-cm-long PPLN/W with a Sagnac configuration [21, 24]. The pump power coupled to the PPLN/W was approximately 1.0 mW for both the clockwise and counterclockwise directions. We used volume holographic gratings (VHGs) with a 32-GHz FWHM (i.e., in accordance with the phase-matching bandwidth of the SFG-BSA unit) to narrow the bandwidths of the signal and idler photons. Table 2 summarizes the average photon numbers per mode ( $\mu$ ), Klyshko efficiencies [44] ( $h$ ), and the transmittance ( $T$ ) in the optical circuit before the SFG-BSA including the coupling efficiencies to the SFG-BSA. We employed a flip mirror (not shown) just before the SFG-BSA to evaluate the input quantum states from EPS I and II. The detection rate of the entangled photon pairs for each EPS was measured to be 1.1 MHz.

**Table 2 Parameters of EPS I and EPS II.**

	EPS I			EPS II		
	$\mu_1$	$h_1$	$T_1$	$\mu_2$	$h_2$	$T_2$
H	0.060	0.097	0.44	0.080	0.070	0.56
V	0.050	0.11	0.48	0.061	0.10	0.57

## Theoretical SFG efficiency

The PPLN/W3 used for SFG possesses a crystal length of  $L=6.3$  cm and a core diameter of  $7.2 \mu\text{m} \times 8.0 \mu\text{m}$  [19]. The normalized SHG efficiency was measured to be  $\eta_{\text{SHG}} = 28 \%/ \text{W}/\text{cm}^2$  using a narrow-band CW laser light. The SFG conversion efficiency for single-photon inputs can be estimated using the following equation [6, 17]:

$$\eta_{\text{SFG}}^{\text{th}} = \frac{\eta_{\text{SHG}}}{2} \times \frac{hc}{\lambda} \times \frac{\Delta\nu L}{\text{tbp}}, \quad (4)$$

where  $\Delta\nu$  is the spectral acceptance of the crystal and  $\text{tbp}$  is the time-bandwidth product of the SFG photon. By substituting the experimental values of  $\lambda = 1550$  nm,  $\Delta\nu = 2.47 \times 10^2$  GHz-cm and  $\text{tbp} = 0.67$ , we obtain  $\eta_{\text{SFG}}^{\text{th}} = 4.19 \times 10^{-8}$ . The SFG efficiency for SPDC photons is estimated by considering the overlap integral among

the spectral distributions of the input photons  $\phi_{a(b)}(\lambda_{a(b)})$ , and the normalized phase-matching function of PPLN/W3  $\eta(\lambda_a, \lambda_b)$  as [17]

$$\eta_{\text{SFG}}^{\text{eff}} = \eta_{\text{SFG}}^{\text{th}} \int \int \phi_a(\lambda_a) \phi_b(\lambda_b) \eta(\lambda_a, \lambda_b) d\lambda_a d\lambda_b. \quad (5)$$

From the measured results, when  $\phi_a(\lambda_a)$ ,  $\phi_b(\lambda_b)$ ,  $\eta(\lambda_a, \lambda_b)$  are calculated as Gaussians with FWHM of 0.25, 0.27, and 0.32 nm, respectively, we obtain  $\eta_{\text{SFG}}^{\text{eff}} = 2.70 \times 10^{-8}$ , which is close to the experimental values of  $\eta_{\text{SFG}}^H = 2.31 \times 10^{-8}$  and  $\eta_{\text{SFG}}^V = 2.35 \times 10^{-8}$ .

## Widths of coincidence windows

The width of the coincidence window is determined according to the timing jitters of the SNSPDs. The SFG photon  $c$  at 780 nm is detected by D1, whose timing jitter is 190 ps. The telecom photons are detected by D2, D3, D4, and D5, whose timing jitters are 48, 98, 64, and 162 ps, respectively (Fig. 2). The largest timing jitter among the three-fold coincidences is given according to the convolution of the timing jitters of D1, D3, D5, and the coherence time of SPDC photons of 14 ps as 269 ps. We used the coincidence window with  $\tau_w=448$  ps, which covers 96% of the signal events.

## Theoretical analysis

We discuss the validity of the experimentally obtained visibilities, using a realistic model and independently measured experimental parameters. We considered the dark counts in D1 and the multiple photons generated in EPS I and EPS II using the following approach. First, we considered the events where a maximum of three photon pairs is produced between EPS I and EPS II as an input. Then, we performed the SFG operation after photons  $a$  and  $b$  experienced system losses. We assume that the coupling constant  $\chi$  in Eq. (1) is dependent on the inputs' polarization, which is defined as  $\chi_{H(V)}$  for  $H$ -( $V$ -) polarized input, respectively. In this model, a maximum of one SFG photon is produced, which is detected by a threshold detector D1. Conditioned by the detection signal from D1, polarization correlation measurements were performed using D2, D3, D4, and D5. The three-fold coincidence probability is given by  $P_{ij}^{\text{SFG}}(\theta_1, \theta_2)$  with  $i, j \in \{H, V\}$ . Here, Z-basis and X-basis are expressed by  $(\theta_1, \theta_2) = (0, 0)$  and  $(\pi/4, \pi/4)$ , respectively. For example,  $P_{HV}^{\text{SFG}}(\pi/4, \pi/4)$  corresponds to the coincidence probability where  $D$ - and  $A$ -polarized photons are detected by D3 and D4 according to the heralding signal from D1, respectively. We also consider the event where the heralding signal from D1 is caused by the dark counts. Because the dark count probability at D1 is given by  $R_d \times \tau_w$ , the coincidence detection probability between photons  $d$  and  $e$  heralded by the dark count at D1 is given by  $R_d \tau_w (P_{ij}^{\text{Accd}}(\theta_1, \theta_2) - P_{ij}^{\text{SFG}}(\theta_1, \theta_2))$ , where  $P_{ij}^{\text{Accd}}(\theta_1, \theta_2)$  is the accidental coincidence detection probability between photons  $d$  and  $e$ . The visibilities of the swapped state are calculated using the above coincidence probabilities as

$$V_Z^{\text{th}} = \frac{P_{HH}(0, 0) + P_{VV}(0, 0) - P_{HV}(0, 0) - P_{VH}(0, 0)}{P_{HH}(0, 0) + P_{VV}(0, 0) + P_{HV}(0, 0) + P_{VH}(0, 0)} \quad (6)$$



and

$$V_X^{\text{th}} = \frac{P_{HV}(\frac{\pi}{4}, \frac{\pi}{4}) + P_{VH}(\frac{\pi}{4}, \frac{\pi}{4}) - P_{HH}(\frac{\pi}{4}, \frac{\pi}{4}) - P_{VV}(\frac{\pi}{4}, \frac{\pi}{4})}{P_{HV}(\frac{\pi}{4}, \frac{\pi}{4}) + P_{VH}(\frac{\pi}{4}, \frac{\pi}{4}) + P_{HH}(\frac{\pi}{4}, \frac{\pi}{4}) + P_{VV}(\frac{\pi}{4}, \frac{\pi}{4})}, \quad (7)$$

where  $P_{ij}(\theta_1, \theta_2) := P_{ij}^{\text{SFG}}(\theta_1, \theta_2)(1 - R_d\tau_W) + R_d\tau_W P_{ij}^{\text{Acid}}(\theta_1, \theta_2)$ . The detailed calculation and the theoretical model are presented in S1 in Supplementary information.

By substituting  $\eta_{\text{SFG}}^H = 2.31 \times 10^{-8}$ ,  $\eta_{\text{SFG}}^V = 2.35 \times 10^{-8}$ , and the parameters in Tables 1 and 2, the theoretically calculated visibility values are  $V_Z^{\text{th}} = 0.78$  and  $V_X^{\text{th}} = 0.76$ , respectively, which exhibit a good agreement with the experimentally observed visibilities  $V_Z = 0.833(92)$  and  $V_X = 0.706(121)$ .

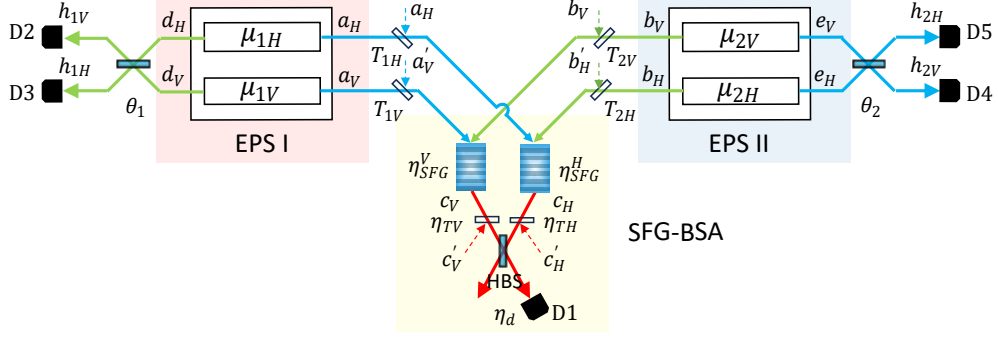


**Fig. S1 Realistic model of SFG-based entanglement swapping.** Each EPS consists of two photon pair sources. The polarization correlation measurements on the swapped state are performed by the beamsplitters in the polarization DOF followed by photon detections using threshold detectors.

## Supplementary information

### 1 Model of SFG-based entanglement swapping

We present the detailed procedure to calculate the theoretical visibility of the swapped state using the realistic model shown in Fig. S1. We assume that each EPS consists of two two-mode squeezed vacua, and the initial state is given by  $|\psi_{in}\rangle = |\psi\rangle_{ad} \otimes |\psi\rangle_{be}$ , where

$$|\psi\rangle_{ad} := \sqrt{1 - \gamma_{1H}^2} \sum_{k=0}^{\infty} \frac{1}{k!} (\gamma_{1H} \hat{a}_H^\dagger \hat{d}_H^\dagger)^k |\text{vac}\rangle \otimes \sqrt{1 - \gamma_{1V}^2} \sum_{l=0}^{\infty} \frac{1}{l!} (\gamma_{1V} \hat{a}_V^\dagger \hat{d}_V^\dagger)^l |\text{vac}\rangle \quad (\text{S1})$$

and

$$|\psi\rangle_{be} := \sqrt{1 - \gamma_{2H}^2} \sum_{k=0}^{\infty} \frac{1}{k!} (\gamma_{2H} \hat{b}_H^\dagger \hat{e}_H^\dagger)^k |\text{vac}\rangle \otimes \sqrt{1 - \gamma_{2V}^2} \sum_{l=0}^{\infty} \frac{1}{l!} (\gamma_{2V} \hat{b}_V^\dagger \hat{e}_V^\dagger)^l |\text{vac}\rangle. \quad (\text{S2})$$

Here, the photon-number distributions are characterized by the average photon numbers as  $\gamma_{1H} = \sqrt{\mu_{1H}/(1 + \mu_{1H})}$  for example. Hereafter, we consider the events where up to a total of three photon pairs are produced in  $|\psi_{in}\rangle$ . Optical losses in modes  $a_H$ ,  $a_V$ ,  $b_H$  and  $b_V$  are simulated by virtual beamsplitters (BSs) whose transmittance are  $T_{1H}$ ,  $T_{1V}$ ,  $T_{2H}$  and  $T_{2V}$ , respectively. For example, the optical loss operation in mode  $a_H$  is represented by

$$\mathcal{L}_{a'_H}(|\psi_{in}\rangle\langle\psi_{in}|) = \text{Tr}_{a'_H}[\hat{U}_{a'_H}|\psi_{in}\rangle\langle\psi_{in}| \otimes |\text{vac}\rangle\langle\text{vac}|_{a'_H} \hat{U}_{a'_H}^\dagger], \quad (\text{S3})$$

where  $a'_H$  is an ancillary mode and  $\hat{U}_{a'_H}$  is the unitary operator of the BS whose transmittance is  $T_{1H}$ , which satisfies  $\hat{U}_{a'_H} \hat{a}_H^\dagger \hat{U}_{a'_H}^\dagger = \sqrt{T_{1H}} \hat{a}_H^\dagger + \sqrt{1-T_{1H}} \hat{a}'_H^\dagger$  and  $\hat{U}_{a'_H} |\text{vac}\rangle = |\text{vac}\rangle$ . The quantum state after experiencing the optical losses is given by

$$\hat{\rho}_L = \mathcal{L}_{a'_H} \circ \mathcal{L}_{a'_V} \circ \mathcal{L}_{b'_H} \circ \mathcal{L}_{b'_V} (|\psi_{in}\rangle\langle\psi_{in}|). \quad (\text{S4})$$

Since the threshold detectors are used in the later photon detection, we only need to consider the subspace of  $\hat{\rho}_L$  where the number of photons in  $|\psi_{in}\rangle$  and  $\langle\psi_{in}|$  are equal. As a next step, the SFG operation is performed on the photons in modes  $a_H$ ,  $a_V$ ,  $b_H$  and  $b_V$ . We note that Eq. (2) is not enough to express the SFG operation in this model, since it is derived under the condition the number of the input photons is at most two. Thus, we need to derive the SFG operation on the three-photon inputs. Moreover, we consider that the coupling constant  $\chi$  in Eq. (1) is dependent on the polarization of the inputs, which we define  $\chi_{H(V)}$  for  $H(V)$ -polarized input, respectively. Considering only the first order of  $\chi_H$  and  $\chi_V$  in  $U = e^{-i\hat{H}'\tau/\hbar}$ , the corresponding operation is approximated by

$$U \sim -i\hat{H}'\tau/\hbar = \tau(\chi_H \hat{a}_H \hat{b}_H \hat{c}_H^\dagger + \chi_V \hat{a}_V \hat{b}_V \hat{c}_V^\dagger) - \text{H.c.} \quad (\text{S5})$$

We exemplify the dynamics for SFG operations involving three photons. As the first case, we consider the case where two photons  $\hat{a}_i^\dagger$  and  $\hat{b}_i^\dagger$  in an identical polarization state and photon  $\hat{a}_j^\dagger$  in a polarization orthogonal to them are input e.g.  $\hat{a}_H^\dagger \hat{a}_V^\dagger \hat{b}_H^\dagger |\text{vac}\rangle$ . Performing Eq. (S5), we obtain

$$(-i\hat{H}'\tau/\hbar) \hat{a}_H^\dagger \hat{a}_V^\dagger \hat{b}_H^\dagger |\text{vac}\rangle = \sqrt{\eta_{\text{SFG}}^H} \hat{a}_V^\dagger \hat{c}_H^\dagger |\text{vac}\rangle, \quad (\text{S6})$$

where  $\eta_{\text{SFG}}^H := (\chi_H \tau)^2$ . As the second case, we consider the case where two photons  $(\hat{a}_i^\dagger)^2$  in an identical polarization state and photon  $\hat{b}_j^\dagger$  in a polarization orthogonal to that of photon  $a$  are input. For example,  $(\hat{a}_H^\dagger)^2 \hat{b}_V^\dagger |\text{vac}\rangle$  is transformed into

$$(-i\hat{H}'\tau/\hbar) (\hat{a}_H^\dagger)^2 \hat{b}_V^\dagger |\text{vac}\rangle = 0. \quad (\text{S7})$$

As the third case, we consider the case of the three-photon input in an identical polarization. For example,  $\frac{1}{\sqrt{2}} (\hat{a}_H^\dagger)^2 \hat{b}_H^\dagger |\text{vac}\rangle$  is transformed into

$$(-i\hat{H}'\tau/\hbar) \frac{1}{\sqrt{2}} (\hat{a}_H^\dagger)^2 \hat{b}_H^\dagger |\text{vac}\rangle = \sqrt{\frac{\eta_{\text{SFG}}^H}{2}} (1 - \hat{a}_H^\dagger \hat{a}_H) \hat{a}_H^\dagger (1 - \hat{b}_H^\dagger \hat{b}_H) \hat{c}_H^\dagger |\text{vac}\rangle \quad (\text{S8})$$

$$= \sqrt{2\eta_{\text{SFG}}^H} \hat{a}_H^\dagger \hat{c}_H^\dagger |\text{vac}\rangle, \quad (\text{S9})$$

which shows that the SFG efficiency is doubled compared to the case where  $\hat{a}_H^\dagger \hat{a}_V^\dagger \hat{b}_H^\dagger |\text{vac}\rangle$  is the input. The SFG photons  $c_H$  and  $c_V$  experience optical losses  $\mathcal{L}_{c'_H}$  and  $\mathcal{L}_{c'_V}$ , respectively. The projection of the SFG photon on  $|D\rangle$  and  $|A\rangle$  is simulated by mixing  $c_H$  and  $c_V$  by a virtual HBS in polarization DOF followed by photon

detections by threshold detectors. Since we consider the case where at most one SFG photon is emitted, POVM elements of the projective measurements on  $|D\rangle$  and  $|A\rangle$  are approximated by  $\Pi_c^D \sim \eta_d |D\rangle_c \langle D|_c$  and  $\Pi_c^A \sim \eta_d |A\rangle_c \langle A|_c$ , respectively, where  $\eta_d$  is the quantum efficiency of D1. The unnormalized quantum state after detecting the  $A$ -polarized SFG photon is given by

$$\hat{\rho}_{\text{SFG}} = \text{Tr}_{a_H, a_V, b_H, b_V, c_H, c_V} [\Pi_c^A \mathcal{L}_{c'_H} \circ \mathcal{L}_{c'_V} ((-i\hat{H}'\tau/\hbar)\hat{\rho}_L(-i\hat{H}'\tau/\hbar)^\dagger)]. \quad (\text{S10})$$

Finally, polarization correlation measurements on photon  $d$  and  $e$  are performed. Similar to the projective measurement on the SFG photon,  $H$  and  $V$  polarized components are mixed by virtual BSs in polarization DOF whose transmittance is  $\cos^2 \theta_1$  and  $\cos^2 \theta_2$  for the photons  $d$  and  $e$ , respectively, and are detected by the threshold detectors. We exemplify the POVM element of photon detection at D3 as

$$\hat{\Pi}_{d_H}(\theta_1) = \sum_{n=1}^2 \frac{1}{n!} (1 - (1 - h_{1H})^n) \hat{U}_{\text{BS}}(\theta_1) (\hat{d}_H^\dagger)^n |\text{vac}\rangle \langle \text{vac}| (\hat{d}_H)^n \hat{U}_{\text{BS}}^\dagger(\theta_1). \quad (\text{S11})$$

Here the sum of  $n$  is limited to 2, since the maximum number of photons in a single mode is 2 in this model.  $\hat{U}_{\text{BS}}(\theta_1)$  is the unitary operator of the BS, which satisfies  $\hat{U}_{\text{BS}}(\theta_1) \hat{d}_H^\dagger \hat{U}_{\text{BS}}^\dagger(\theta_1) = \cos \theta_1 \hat{d}_H^\dagger + \sin \theta_1 \hat{d}_V^\dagger$  and  $\hat{U}_{\text{BS}}(\theta_1) |\text{vac}\rangle = |\text{vac}\rangle$ . When  $Z(X)$ -basis measurements are performed,  $\theta_1$  and  $\theta_2$  are set to be  $0(\pi/4)$ , respectively. For example, the coincidence probability between D3 and D5 heralded by D1 is given by

$$P_{HH}^{\text{SFG}}(\theta_1, \theta_2) = \text{Tr}[\hat{\Pi}_{d_H}(\theta_1) \hat{\Pi}_{e_H}(\theta_2) \hat{\rho}_{\text{SFG}}]. \quad (\text{S12})$$

Here the subscript “ $HH$ ” comes from the fact that D3 and D5 detect  $H$ -polarized components after the FPBSs. (See Fig. 2 in the manuscript)

In addition to the influence of the multi-photon creation considered above, there are accidental coincidences caused by the dark counts of the detectors. Since the dark count probabilities of D2, D3, D4, and D5 are sufficiently smaller than their photon detection probabilities, only the effect of the dark count of D1 is considered in this model. The coincidence probability between D3 and D5 heralded by the dark count in D1 is given by  $R_d \tau_W (P_{HH}^{\text{Acid}}(\theta_1, \theta_2) - P_{HH}^{\text{SFG}}(\theta_1, \theta_2))$ , where  $R_d \times \tau_W$  is the dark count probability of D1, and

$$P_{HH}^{\text{Acid}}(\theta_1, \theta_2) = \text{Tr}[\hat{\Pi}_{d_H}(\theta_1) \hat{\Pi}_{e_H}(\theta_2) \text{Tr}_{a_H, a_V, b_H, b_V} [|\psi_{in}\rangle \langle \psi_{in}|]] \quad (\text{S13})$$

is the accidental coincidence between D3 and D5. By using Eq. (S12) and Eq. (S13), the visibilities in  $Z$  and  $X$  basis are respectively given by

$$V_Z^{\text{th}} = \frac{P_{HH}(0, 0) + P_{VV}(0, 0) - P_{HV}(0, 0) - P_{VH}(0, 0)}{P_{HH}(0, 0) + P_{VV}(0, 0) + P_{HV}(0, 0) + P_{VH}(0, 0)} \quad (\text{S14})$$

and

$$V_X^{\text{th}} = \frac{P_{HV}(\frac{\pi}{4}, \frac{\pi}{4}) + P_{VH}(\frac{\pi}{4}, \frac{\pi}{4}) - P_{HH}(\frac{\pi}{4}, \frac{\pi}{4}) - P_{VV}(\frac{\pi}{4}, \frac{\pi}{4})}{P_{HV}(\frac{\pi}{4}, \frac{\pi}{4}) + P_{VH}(\frac{\pi}{4}, \frac{\pi}{4}) + P_{HH}(\frac{\pi}{4}, \frac{\pi}{4}) + P_{VV}(\frac{\pi}{4}, \frac{\pi}{4})}, \quad (\text{S15})$$

**Table S1** The experimental parameters necessary for calculating  $V_Z^{\text{th}}$  and  $V_X^{\text{th}}$ .

*	$\mu_{1*}$	$h_{1*}$	$T_{1*}$	$\mu_{2*}$	$h_{2*}$	$T_{2*}$	$\eta_{\text{SFG}}^*$	$\eta T^*$	$\eta_d$
H	0.060	0.097	0.44	0.080	0.070	0.56	$2.31 \times 10^{-8}$	0.43	0.85
V	0.050	0.11	0.48	0.061	0.10	0.57	$2.35 \times 10^{-8}$	0.40	0.85

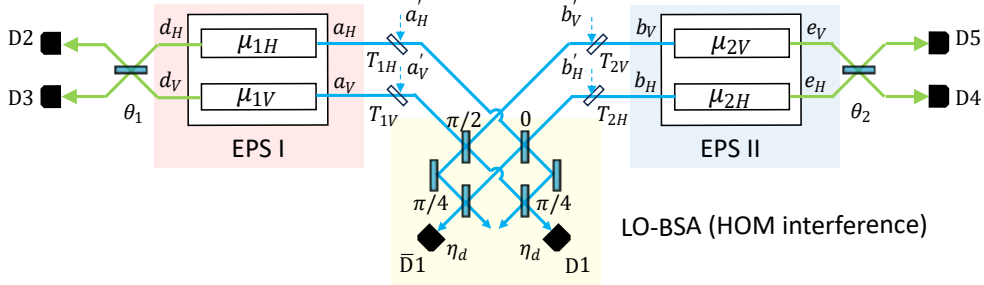


**Fig. S2** Model of linear optical entanglement swapping. Linear optical BSA is realized by mixing the  $H$  and  $V$  polarization components of the input photons with a polarization beamsplitter and then performing projective measurements in the  $X$  basis.

where  $P_{ij}(\theta_1, \theta_2) := P_{ij}^{\text{SFG}}(\theta_1, \theta_2)(1 - R_d\tau_W) + R_d\tau_W P_{ij}^{\text{Acid}}(\theta_1, \theta_2)$  with  $i, j \in \{H, V\}$ . Here,  $V_Z^{\text{th}}$  and  $V_X^{\text{th}}$  are functions of the experimental parameters summarized in Table S1. Substituting the experimental parameters, we obtain  $V_Z^{\text{th}} = 0.78$  and  $V_X^{\text{th}} = 0.76$ , respectively.

## 2 Comparison of SFG-BSA and linear optical BSA

In this section, we quantitatively show the superiority of the SFG-BSA over the linear optical BSA (LO-BSA). We introduce the model of the LO-BSA as shown in Fig. S2. We assume perfect HOM interference and no dark count at the BSA. The unnormalized quantum state just before the BSA is given by  $\hat{\rho}_L$  in Eq. (S4). Here, we assume the symmetric transmittance as  $T_{1H} = T_{1V} = T_{2H} = T_{2V} = T$  for simplicity. The photons in modes  $a$  and  $b$  are then mixed by a PBS, which is simulated by mixing the  $H$ - and  $V$ -polarized components of the photons using two beamsplitters  $\hat{U}_{\text{BS}}^H(0)$  and  $\hat{U}_{\text{BS}}^V(\pi/2)$ , respectively as

$$\hat{\rho}_{\text{PBS}} = (\hat{U}_{\text{BS}}^H(0) \otimes \hat{U}_{\text{BS}}^V(\pi/2))\hat{\rho}_L(\hat{U}_{\text{BS}}^H(0) \otimes \hat{U}_{\text{BS}}^V(\pi/2))^\dagger, \quad (\text{S16})$$

where  $\hat{U}_{\text{BS}}^H(0)$  and  $\hat{U}_{\text{BS}}^V(\pi/2)$  satisfy  $\hat{U}_{\text{BS}}^H(0)\hat{a}_H^\dagger(\hat{U}_{\text{BS}}^H(0))^\dagger = \hat{a}_H^\dagger$ ,  $\hat{U}_{\text{BS}}^H(0)\hat{b}_H^\dagger(\hat{U}_{\text{BS}}^H(0))^\dagger = \hat{b}_H^\dagger$ ,  $\hat{U}_{\text{BS}}^V(\pi/2)\hat{a}_V^\dagger(\hat{U}_{\text{BS}}^V(\pi/2))^\dagger = \hat{b}_V^\dagger$ ,  $\hat{U}_{\text{BS}}^V(\pi/2)\hat{b}_V^\dagger(\hat{U}_{\text{BS}}^V(\pi/2))^\dagger = \hat{a}_V^\dagger$  and  $\hat{U}_{\text{BS}}^H(0)|\text{vac}\rangle = \hat{U}_{\text{BS}}^V(\pi/2)|\text{vac}\rangle = |\text{vac}\rangle$ . Finally, the four-fold coincidences among D1,  $\bar{D}1$ , (D2 or D3) and (D4 or D5) are measured. Here,  $A$ - and  $D$ -polarized components are respectively

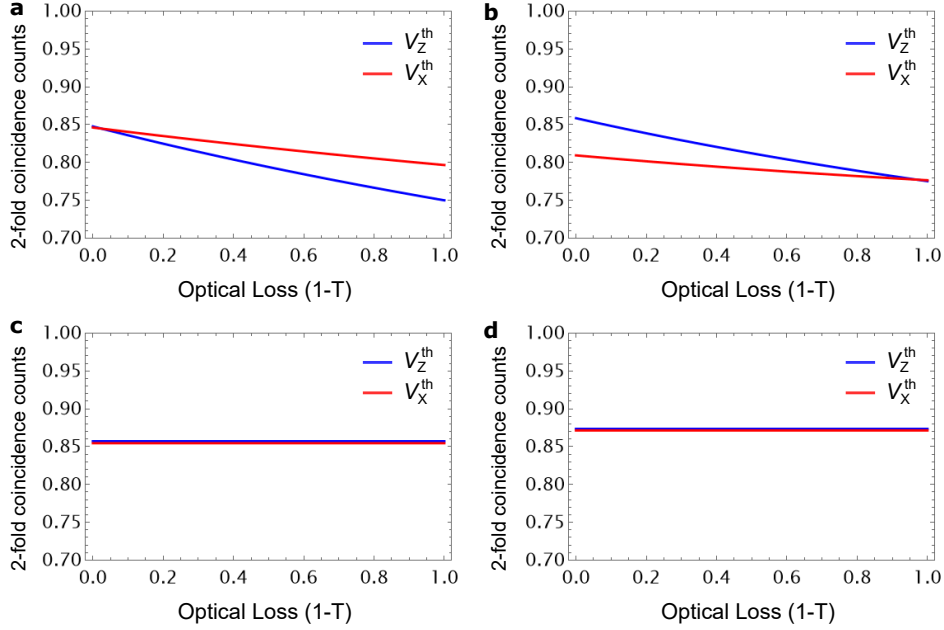


**Fig. S3** Visibilities versus optical loss. **a,b** Entanglement swapping by using LO-BSA with **a**  $h_{1H} = h_{1V} = h_{2H} = h_{2V}$  and **b**  $h_{1H} = h_{1V} = h_{2H} = h_{2V}$ . **c,d** Entanglement swapping using SFG-BSA with **c**  $h_{1H} = h_{1V} = h_{2H} = h_{2V} = 1$  and **d**  $h_{1H} = h_{1V} = h_{2H} = h_{2V} = 0.1$ .

detected by D1 and  $\bar{D}1$  whose quantum efficiencies are  $\eta_d$ . For example, the four-fold coincidence probability among D1,  $\bar{D}1$ , D3 and D5 is given by using the POVM elements defined in Eq. (S11) as

$$P_{HH}^{\text{lin}}(\theta_1, \theta_2) = \text{Tr}[\hat{\Pi}_{dH}(\theta_1)\hat{\Pi}_{eH}(\theta_2)\hat{\Pi}_{bH}(\pi/4)\hat{\Pi}_{aV}(\pi/4)\hat{\rho}_{\text{PBS}}]. \quad (\text{S17})$$

The visibilities of the swapped state are calculated by replacing  $P_{ij}(\theta_1, \theta_2)$  in Eqs. (S14) and (S15) with  $P_{ij}^{\text{lin}}(\theta_1, \theta_2)$ .

In the following, we assume that the average photon number of each two-mode squeezed vacuum is the same as  $\mu_{1H} = \mu_{1V} = \mu_{2H} = \mu_{2V} = 0.05$  and the photon detection probabilities at the LO-BSA are unity as  $\eta_d = 1$  for simplicity. The visibilities  $V_Z^{\text{th}}$  and  $V_X^{\text{th}}$  versus optical loss  $(1 - T)$  with  $h_{1H} = h_{1V} = h_{2H} = h_{2V} = 1$  and  $h_{1H} = h_{1V} = h_{2H} = h_{2V} = 0.1$  are plotted in Fig. S3a and b, respectively. The visibilities decrease as the photon losses increase. This is because the portion of fake success events caused by two photons from one EPS to enter the LO-BSA and be a coincidence between D1 and  $\bar{D}1$  increases as the photon losses increase.

The visibilities obtained by the SFG-BSA *without* dark counts are calculated by replacing  $P_{ij}(\theta_1, \theta_2)$  in Eqs. (S14) and (S15) with  $P_{ij}^{\text{SFG}}(\theta_1, \theta_2)$ . Here, we assume  $\mu_{1H} = \mu_{1V} = \mu_{2H} = \mu_{2V} = 0.05$ ,  $T_{1H} = T_{1V} = T_{2H} = T_{2V} = T$  and  $\eta_{TH} = \eta_{TV} = \eta_d = 1$  as in the case of the LO-BSA. The visibilities  $V_Z^{\text{th}}$  and  $V_X^{\text{th}}$  versus optical loss  $(1 - T)$

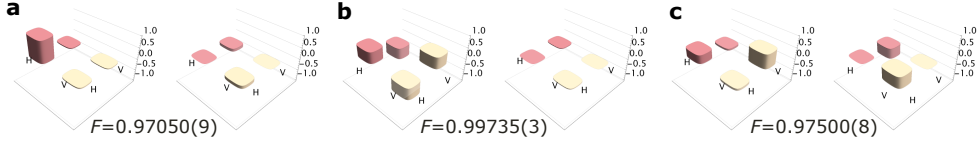


**Fig. S4 Input polarization states.** **a, b, c** Density matrices of the  $H$ -,  $A$ -, and  $R$ -polarized states, respectively.

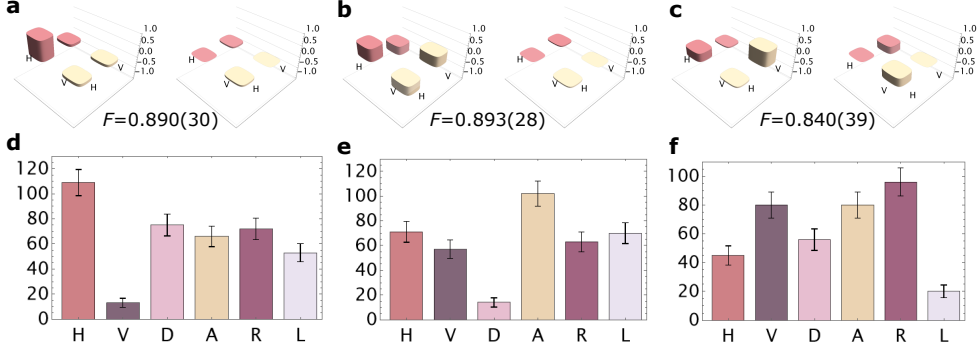


**Fig. S5 Teleported states and raw detection counts.** **a, b, c** Density matrices of the teleported states for the  $H$ -,  $A$ -, and  $R$ -polarized input states, respectively. **d, e, f** Raw detection counts of the teleported photons for the  $H$ -,  $A$ -, and  $R$ -polarized input states, respectively.

with  $h_{1H} = h_{1V} = h_{2H} = h_{2V} = 1$  and  $h_{1H} = h_{1V} = h_{2H} = h_{2V} = 0.1$  are plotted in Fig. S3b and d, respectively. We see that the visibilities are insensitive to the optical losses. This is because the fake success events related to the optical losses, which occur in the LO-BSA, are rejected by the SFG-BSA. As a result, the visibilities remain high despite the effects of optical losses.

### 3 Experimental results of SFG-based quantum teleportation

We show all density matrices and raw counts obtained in the quantum teleportation experiment using SFG-BSA. The density matrices of the input states are shown in Fig. S4. The density matrices and raw counts of the teleported states are shown in Fig. S5 a-c and d-f, respectively.

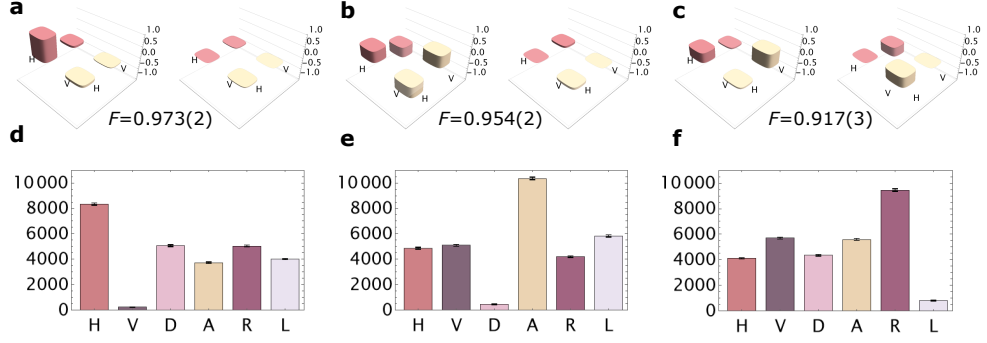


**Fig. S6 Output states and raw detection counts.** **a, b, c** Density matrices of the output states after the QFC for the  $H$ -,  $A$ -, and  $R$ -polarized input states, respectively. **d, e, f** Raw detection counts of the output photons after the QFC for the  $H$ -,  $A$ -, and  $R$ -polarized input states, respectively.

## 4 SFG-based quantum teleportation with large-photon-number inputs

We use coherent light with an average photon number of  $7.5 \times 10^4$  to prepare the input states and perform the quantum teleportation experiment. We show the density matrices and raw counts of the output states in Fig. S6. The fidelities of the output states for  $H$ -,  $A$ - and  $R$ -polarized inputs are 0.973(2), 0.954(2) and 0.917(3), respectively. Interestingly, unlike the case of the linear optical BSA, we observe the “quantum-teleportation-like” operation even if a number of multiple photons are contained in the input coherent light as reported in Ref. [5]. This result can be interpreted as follows. Assuming that the average intensities of the  $H$ - and  $V$ -polarized portion of the input coherent light in mode  $b$  are respectively given by  $|\alpha|^2$  and  $|\beta|^2$ , where the polarization is expressed as  $(\alpha H + \beta V)/\sqrt{|\alpha|^2 + |\beta|^2}$ , and are sufficiently large,  $\hat{b}_{H(V)}$  in Eq. (1) in the manuscript is replaced with  $\alpha(\beta) \in \mathbb{C}$ , respectively, as

$$\hat{H}_{\text{QFC}} = i\hbar\chi(\alpha\hat{a}_H\hat{c}_H^\dagger + \beta\hat{a}_V\hat{c}_V^\dagger) + \text{H.c.}, \quad (\text{S18})$$

which corresponds to the Hamiltonian of the quantum frequency conversion (QFC) [32–34], between modes  $a$  and  $c$ . Here, the input light in mode  $b$  is regarded as pump light. The unitary transformation  $\hat{U}_{\text{QFC}} = e^{-i\hat{H}_{\text{QFC}}\tau/\hbar}$  of  $\hat{a}_{H(V)}$  is represented by [45]

$$\hat{U}_{\text{QFC}}\hat{a}_{H(V)}\hat{U}_{\text{QFC}}^\dagger = \cos(|\alpha(\beta)|\chi\tau)\hat{a}_{H(V)} + e^{i\arg\alpha(\beta)}\sin(|\alpha(\beta)|\chi\tau)\hat{c}_{H(V)}. \quad (\text{S19})$$

In the weak pump regime where  $|\alpha(\beta)|\chi\tau \ll 1$ , the right hand side of Eq. (S19) is approximated by  $\hat{a}_{H(V)} + \sqrt{\eta_{\text{SFG}}}\alpha(\beta)\hat{c}_{H(V)}$ . Thus, after the QFC followed by the detection of a  $D$ -polarized SFG photon in mode  $c$ , we obtain  ${}_c\langle D|\hat{U}_{\text{QFC}}|\Phi^+\rangle_{ad} \propto \alpha|H\rangle_d + \beta|V\rangle_d$ , which shows that the polarization information of the input coherent light is transferred to photon  $d$ . We emphasize that the above dynamics is different



from the quantum teleportation. Therefore, in the strong pump regime, the conversion efficiency is no longer proportional to the pump intensity, and the situation is rather similar to the polarization insensitive QFC [45–47] where no polarization information of the input (pump) light remains in the output photon.